Use of emission-line intensities for a self-consistent determination of the particle densities in a transient plasma

L. Gregorian, V. A. Bernshtam, E. Kroupp, G. Davara,* and Y. Maron
Faculty of Physics, Weizmann Institute of Science, Rehovot 76100, Israel
(Received 11 June 2002; published 15 January 2003)

A method for a self-consistent determination of the time history of the electron density, electron temperature, and ionic charge-state composition in a multicomponent plasma, using time-dependent measurements and calculations of absolute emission-line intensities, is presented. The method is applied for studying the properties of an imploding gas-puff *Z*-pinch plasma that contains several oxygen ions up to the fifth ionization stage. Furthermore, by using intensity ratios of lines from different ion species, the electron temperature was determined with a much improved accuracy, in comparison to previous spectroscopic studies of the same plasma. The ion-density history obtained, together with the known time-dependent radial boundaries of the plasma shell, allowed for tracking the rise in time of the mass swept by the magnetic field during the implosion.

DOI: 10.1103/PhysRevE.67.016404 PACS number(s): 52.58.Lq, 52.25.−b

I. INTRODUCTION

It is known that measurements of spectral line intensities are highly useful for the diagnostics of dense and hot plasmas [1]. However, interpretation of spectroscopic data may be complicated and prone to misleading conclusions for plasmas that are not in ionization or a hydrodynamic steady state. An important example is imploding plasmas, or more specifically a *Z*-pinch plasma [2,3], which is a cylindrical plasma that implodes radially inward under azimuthal magnetic fields produced by a current in the axial direction.

In such a plasma, since the implosion occurs over a time scale comparable to the ionization times of the ions, the level-population densities in a given plasma region viewed by the spectroscopic system vary in time both due to the ionization processes and due to the flow of ions of different charge states into and out of this region. Also, at each radial position the electron density n_e varies in time due to ionization and plasma compression, and the electron temperature T_e varies due to the time-dependent heating and cooling processes. It is, therefore, highly important to formulate methods for a self-consistent determination of these parameters and the charge-state distribution as a function of time; for example, by using time-dependent line intensities observed at any given position (radius in the present study) of the plasma.

The use of line intensities for the determination of the plasma parameters can be particularly important since other spectroscopic methods may not be useful. For example, the determination of n_e from Stark broadening may be impossible because of the opacity and ion-velocity effects on the line shapes [4]. The use of the Thompson scattering technique [5] for the determination of n_e and n_i may also be limited due to the difficulties in the data interpretation for certain conditions of multispecies plasmas. In view of such problems, it is evidently difficult to suggest a data-analysis method that can be useful for a broad range of parameters; a realistic approach would be to examine the parameter range for a specific situation in an attempt to elucidate an appropriate procedure for the determination of the plasma properties.

Here, we describe the use of line intensities from various ion species in order to determine in a self-consistent way the histories of the electron and ion densities, the charge-state composition, and the electron temperature in a moderate density, CO_2 *Z*-pinch plasma. Time-dependent, collisional-radiative (CR) calculations [6] are used to analyze the data. The opacity effects are accounted for by using the escape-probability approximation [7]. The analysis method is based on the dependence of the ratio between the population of an excited state of a certain ion species to the total density of that species on the electron density, and on the dependence of level-population ratios between excited states of different charge-state ions, residing at the same plasma region, on the electron temperature. It should be emphasized that the calculation procedures described here can be used for studying the plasma properties for any atomic or molecular ions.

In Sec. II we describe the gas-puff *Z*-pinch experiment and the spectroscopic measurements. The data-analysis method, where two independent approaches for the determination of n_e are employed, is presented in Sec. III. Also given in Sec. III is a discussion on the uncertainties of the analysis, thus allowing for a detailed comparison with the results of other methods given in our separate studies [8,9]. The calculation of the imploding-plasma mass, based on the particle densities obtained, is described in Sec. IV.

II. EXPERIMENT AND MEASUREMENTS

The experiment and the diagnostics used for the measurements are described in Refs. [10,11]. In brief, the annular plasma is formed and imploded by a 5-kJ, 1-μs capacitor-bank-driven discharge circuit, with the peak plasma compression occuring at $t \sim 620$ ns relative to the beginning of the discharge. The initial plasma outer radius is $\simeq 20$ mm, and the axial plasma length (anode-cathode gap) is 14 mm. The diagnostic system used here consists of a 1.3-m near-uv spectrometer and a high-speed streak camera, yielding tem-

*Present address: Orbotech Ltd., Yavne, Israel.

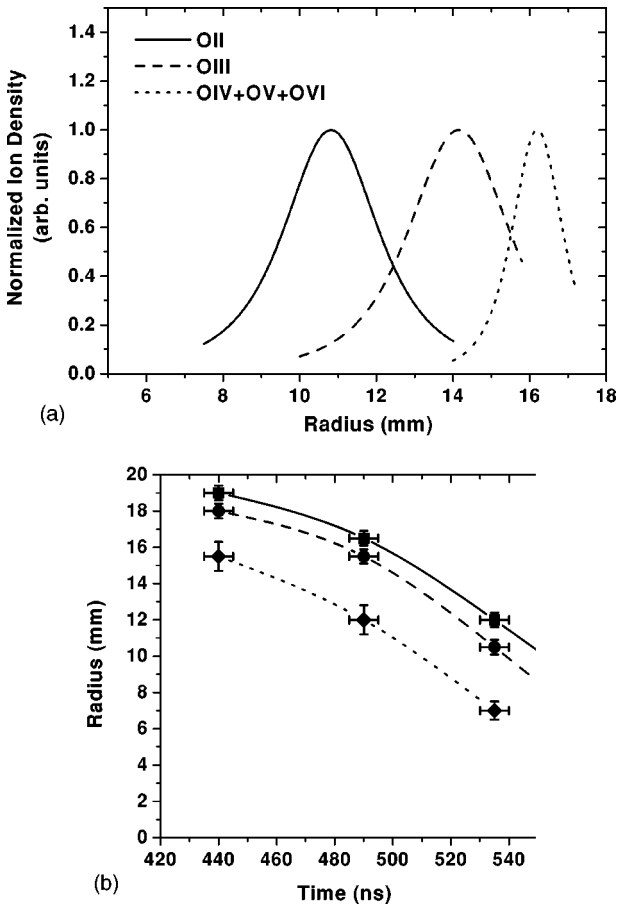

FIG. 1. (a) Radial distribution of oxygen charge states in the plasma shell (spline over experimental points) at $t=490$ ns. Each curve is scaled to unity at its peak experimental point (evidently this figure does not yield the relative abundance of the charge states). (b) The time-dependent boundaries of the imploding shell, $R_{out}(t)$ (solid line) and $R_{in}(t)$ (dashed line), and the inner boundary of the entire plasma column, $R_{min}(t)$ (dotted line).

poral and spatial resolutions of 1 ns and 0.5 mm, respectively.

Throughout the implosion the plasma ionizes continuously, and line spectra of oxygen up to O VI are observed. The charge-state radial distribution in the plasma was studied previously [10], where it was found that at each instant during the implosion until $t\simeq 570$ ns into the current pulse, the higher charge-state ions reside at larger radii than the lower charge-state ions, as shown in Fig. 1(a). This observation was explained by an ionization wave, propagating radially inward faster than the plasma particles. This charge-state distribution was recently used for the determination of the electron temperature $T_e(r,t)$ [8], as briefly described in Sec. III B below.

The radial distribution of the charge-state densities can be used to define the plasma boundaries, as given in Fig. 1(b). The inner radius of the plasma $R_{min}(t)$ is defined as the instantaneous radial position of the peak density of the singly charged ions. The outer radius $R_{out}(t)$ is defined as the instantaneous radial position at which the peak line intensity from the highest charge state is observed. It should be noted that at each instant the total light intensity, observed at a radius $\simeq 0.5$ mm larger than $R_{out}(t)$, was found to be orders of magnitude lower than in the plasma [10], indicating that all the plasma mass is involved in the implosion. We also note that $R_{out}(t)$ is the peak position of the measured magnetic-field radial distribution [12].

In this paper we mainly address the outer region of the plasma shell, here referred to as ''the imploding shell.'' This region is characterized by a density that is significantly higher than the rest of the plasma (as obtained from continuum radiation measurements [9]), and by the highest radial velocities of ions [10], and it contains 70–80 % of the plasma mass. Based on these criteria, the imploding-shell inner boundary $R_{in}(t)$ is defined [see Fig. 1(b)]. The imploding shell evidently contains the highest charge states in the plasma. In more detail, it contains O IV and O V (besides a small fraction of O VI) at $t=490$ ns, and O V and O VI at $t=535$ and $t=565$ ns.

Here, we use time-dependent, end-on observations of absolute line intensities from the imploding plasma at several radial positions, for times between $t\simeq 490$ to 570 ns. For earlier times, line intensities were not sufficient to allow for a reliable data analysis. For the measurements, we use the O IV $3s\,^2S-3p\,^2P$ and $3p\,^2P-3d\,^2D$ lines at 3063.5 and 3411.8 Å, respectively, the O V $3s\,^3S-3p\,^3P$ and $3p\,^1P-3d\,^1D$ lines at 2781.0 and 3144.7 Å, respectively, and the O VI $3s\,^2S-3p\,^2P$ at 3811.35 Å. All lines selected were optically thin [8], therefore the upper-level populations are given by $n_u=I_{ul}/[A_{ul}g_uVK(\lambda)]$, where I_{ul} is the absolute line intensity, A_{ul} is the Einstein coefficient, g_u is the degeneracy of the upper level, and V is the light-emitting plasma volume. $K(\lambda)$ is the wavelength-dependent system sensitivity, determined from the system absolute calibration, obtained for the entire spectral range using a deuterium radiation source of known intensity, and from the light-collection efficiency.

III. DATA ANALYSIS

A. Determination of the electron density

As stated above, the goal of the present analysis is to determine the histories of the electron density and the charge-state composition. The analysis performed here is based on CR calculations in which the electron density, the electron temperature, the initial plasma composition, and the particle time-dependent source functions that simulate the continuous particle supply to the plasma are used as input parameters. In order to examine the sensitivity of the calculation results to the various input parameters, we start the calculations using constant values of n_e and T_e, and a constant number of ions for which the initial conditions (at $t=0$ of the calculations) are such that all particles reside in the ground state of a certain charge-state ion. This particle source is here referred to as ''the δ-source.'' The level populations are calculated for several tens of nanoseconds, since this is the typical range of the ionization times in the plasma. The relevant range of n_e is known from measurements of the continuum radiation [9].

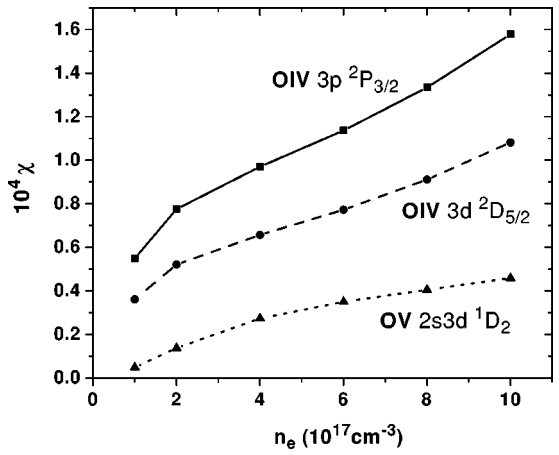

FIG. 2. Typical results for the ratios χ for various upper energy levels of O IV and O V as a function of the electron density, obtained from CR calculations using $T_e=10$ eV and a δ-source (see text) at the ground state of O III at $t=0$. The calculation results shown are for $t=20$ ns. All the upper-level populations are divided by the degeneracy, as throughout the entire paper.

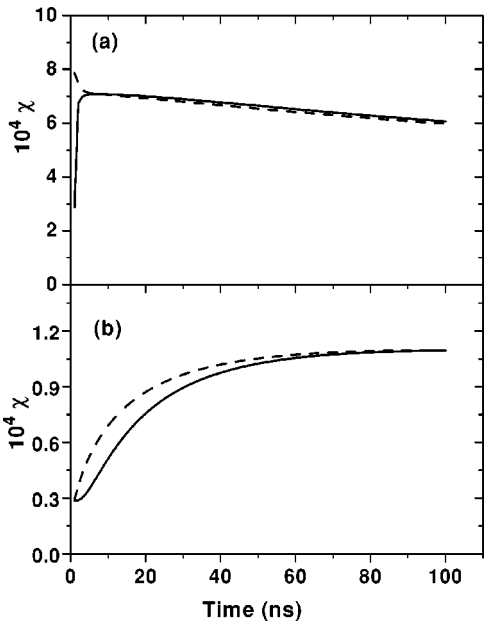

FIG. 3. Calculated ratios $\chi(t)$ for upper energy levels of O IV and O V, obtained using $n_e=4\times10^{17}$ cm^{-3} and $T_e=10$ eV. In the calculations, δ-sources were used at the ground state of O III (solid line) and at the ground state of O IV (dashed line). Results are given for the O IV $3d\ ^2D$ level (a) and for the O V $3d\ ^1D$ level (b).

These CR calculations provide a set of time-dependent upper ionic-level densities $n_u^{\alpha,j}(t)$, the total charge-state densities $n_{tot}^{\alpha}(t)$, and the mean ionic charge $Z(t)$, where α and j are the charge state and the upper level, respectively. Let us define $\chi^{\alpha,j}(n_e,T_e,t)=[n_u^{\alpha,j}/n_{tot}^{\alpha}](t)$. As an example, the dependence of χ^{α} on n_e for different levels of O IV and O V, obtained for a given T_e, t, and a δ-source is shown in Fig. 2. The time dependence of χ^{α}, calculated using typical values of n_e and T_e and different δ-sources is shown in Fig. 3. In this figure, it is seen that χ^{α} for O IV and O V reach nearly constant values after ~ 4 and 25 ns, respectively. The ionization times of O III and of O IV, as observed experimentally, are longer, thus justifying the use of a constant, time-averaged value $\overline{\chi}\pm\Delta\chi$ for the calculations. This is found to be correct for all charge states here studied.

The total ion density for the charge-state α is then calculated from the population of the upper-level j,

$$N_{tot}^{\alpha,j}=\frac{n_u^{\alpha,j}(\text{expt.})}{\overline{\chi^{\alpha}}}, \tag{1}$$

where $\overline{\chi^{\alpha}}$ is a constant value obtained as described above. For the cases where several lines of the same charge-state α are measured, we use averages over the various levels j to obtain a total charge-state density N_{tot}^{α}. The first iteration then gives the oxygen-ion density $N_{tot}^{O}=\Sigma_{\alpha}N_{tot}^{\alpha}$ and the total electron density $N_e^{O}=\Sigma_{\alpha}Z_{\alpha}^{O}N_{tot}^{\alpha,O}$ due to the oxygen ions.

In order to determine the total electron density, one uses the same n_e and T_e as for oxygen for CR calculations of the relative charge-state abundance for carbon (since the gas used is CO_2). Since $N_{tot}^{C}=0.5N_{tot}^{O}$, these calculations yield the absolute carbon-ion charge-state abundance, and the total electron density is then given by $N_e=\Sigma_{\alpha}Z_{\alpha}^{O}N_{tot}^{\alpha,O}+\Sigma_{\beta}Z_{\beta}^{C}N_{tot}^{\beta,C}$, where β is the charge state of the carbon ions and $N_{tot}^{\beta,C}$ is the total density of the charge-state β. Let us define $\delta n_e=(N_e-n_e)/n_e$, where n_e is the input value of the electron density in the CR calculations and N_e is the calculated density. Repeating the calculation procedure iteratively to minimize δn_e, then allows for the determination of the electron density. Given in Table I are the calculation results for O IV, O V, and O VI, obtained using $T_e=10.5$ eV and a δ-source supplied to the O IV ground state, demonstrating the

TABLE I. Example of the iterative calculation procedure described in Sec. III A for the determination of the electron density N_e at $t=490$ ns. Z^{O} and Z^{C} are the mean charge state for oxygen and carbon, respectively, and N_i^{O} is the total oxygen-ion density (n_e is the assumed electron density).

T_e (eV)	n_e (10^{17} cm^{-3})	Z^{O}	Z^{C}	N_i^{O} (10^{17} cm^{-3})	N_e (10^{17} cm^{-3})	δn_e
10.5	3.8	4.1	3.9	0.57	3.45	0.09
	3.7	4.1	3.9	0.58	3.51	0.05
	3.6	4.1	3.9	0.60	3.63	−0.0083
	3.4	4.0	3.9	0.64	3.81	−0.12
	3.0	4.0	3.9	0.75	4.46	−0.49

TABLE II. Summary of results for the plasma parameters at three times during the implosion. $n^{\mathrm{O\ IV}}$-$n^{\mathrm{O\ VII}}$ are the relative densities (normalized to 1) of the charge states O IV-O VII, respectively.

t (ns)	T_e (eV)	N_e (10^{17} cm^{-3})	Z_O	$n^{\mathrm{O\ IV}}$	$n^{\mathrm{O\ V}}$	$n^{\mathrm{O\ VI}}$	$n^{\mathrm{O\ VII}}$
490	10.5	3.6	4.1	0.11	0.67	0.22	0.00
535	12.0	4.0	4.7	0.01	0.31	0.63	0.05
565	13.0	6.0	4.8	0.01	0.26	0.65	0.08

convergence procedure for δn_e for several values of n_e.

Table II gives the results for N_e and the oxygen charge-state composition, determined for three instants during the implosion. Such calculations were performed for the various charge states at different times and radii, giving a complete radial mapping of n_e in the plasma [9].

We note that the use of a constant value of n_e for analyzing the data for each instant in such a rapidly ionizing plasma is possible due to the high rates of the atomic processes. It was verified that the response time of level populations and the population ratios to rapid variations in n_e for the present densities and temperatures is much shorter (1–3 ns) than the observation time interval of $\simeq$10 ns [8].

B. Time dependence of the line intensities

In this section we describe an analysis of the plasma properties that utilizes line emission from two charge states that are similarly abundant in the plasma, as commonly occurs in transient plasmas. The analysis is demonstrated here for the outer (and most dense in this experiment) region of the imploding plasma that contains O V and O VI during the latter stages of the implosion.

In this analysis, we use the measured time-dependent populations n_u of upper levels of transitions of two successive charge-states α and $\alpha+1$ that are similarly abundant at a given time and radial position, yielding the ratio $\gamma_{j,k}^{\alpha,\alpha+1}(\mathrm{expt.})=n_u^{\alpha+1,j}/n_u^{\alpha,k}$, where j and k are levels of the charge-states α and $\alpha+1$, respectively. Time-dependent CR modeling of the plasma at the same radial position is then performed to calculate the ratio $\gamma_{j,k}^{\alpha,\alpha+1}(\mathrm{calc.})$ for the same levels j and k, which is then used to best fit the time-dependent experimental ratio. The calculations are performed iteratively, using various simple functions $n_e(t)$ and $T_e(t)$. For the first iteration, we use for $t=0$ the initial charge-state composition obtained in Sec. III A (Table II), $n_e(t)$ chosen to best fit the data points of N_e (Table I), and $T_e(t)$ chosen to best fit the data points taken from the analysis described in Ref. [8].

The ratio $\gamma^{\alpha,\alpha+1}$, as well as the time-dependent ratio of the total charge-state densities $N_{tot}^{\alpha+1}/N_{tot}^{\alpha}$, are both sensitive to n_e and especially to T_e, resulting from the dependence of the ionization time of the charge-state α on T_e. Therefore, this analysis allows $T_e(t)$ to be determined self-consistently with both $n_e(t)$ and the charge-state composition. This can be further used to examine the accuracy of the results given in Ref. [8], where $T_e(r,t)$ was obtained from upper-level population ratios within the same charge state, that were shown to be insensitive to n_e. It should also be emphasized

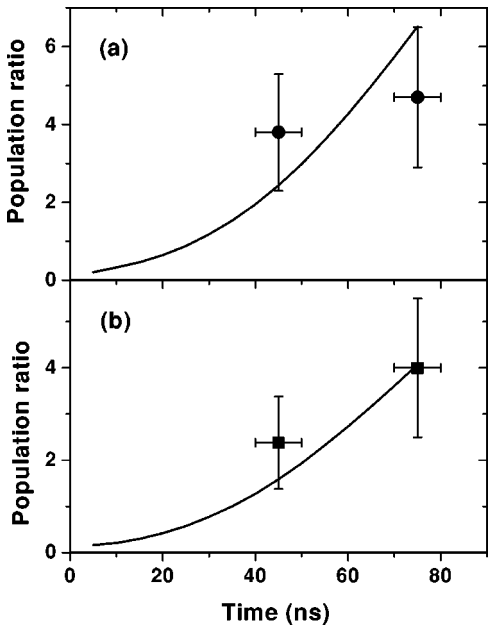

FIG. 4. Experimental and calculated population ratios γ(expt.) and γ(calc.) of the O VI $3p\ ^2P$ to the O V $2s\,3p\ ^3P$ level densities (a) and of the O VI $3p\ ^2P$ to the O V $2s\,3d\ ^1D$ level densities (b). The CR calculations start at $t=0$, corresponding to the experimental time of 490 ns (see text).

that this approach for the analysis is advantageous due to the independence of γ(expt.) on the absolute calibration of the spectroscopic system.

An example of this analysis is given in Fig. 4, where the experimental level-population ratios $3p\ ^2P$ (O VI)/$3p\ ^3P$ (O V) and $3p\ ^2P$ (O VI)/$3d\ ^1D$ (O V), obtained for the time period between $t=490$ and 570 ns, corresponding to the radial positions at $r=16.5$ and $r=8$ mm, respectively, are shown. Also given in Fig. 4 are the best-fit calculations of the ratios γ(calc.), where the starting time for the calculations ($t=0$) corresponds to the experimental time of $t=490$ ns.

Figure 5 gives $n_e(t)$ and $T_e(t)$ obtained iteratively to provide the best fit of the calculated γ(calc.) to γ(expt.). For comparison, also given are the electron density N_e at three instants, obtained in the preceding section, and the data points for T_e given in Ref. [8]. N_e and $n_e(t)$ are found to agree, to within the uncertainty of the absolute calibration (discussed in the following section) that affects the determination of N_e.

$T_e(t)$ is found to be in an excellent agreement with the points obtained in Ref. [8]. Moreover, it should be emphasized that due to the high sensitivity of γ(calc.) to the choice of the function $T_e(t)$, the time-dependent analysis allows for a detailed examination of the time history of T_e, as will be described below.

The calculated time-dependent ion charge-state composition, obtained in the best-fit calculation (Fig. 4), is given in Fig. 6(a). The initial composition (at $t=0$) is obtained from Table II. Figure 6(b) gives the calculated total ion-density history, determined using the relation $n_i(t)=n_e(t)/[\frac{2}{3}Z_O(t)+\frac{1}{3}Z_C(t)]$, where $Z_O(t)$ and $Z_C(t)$ are the mean ion charges obtained from the CR calculations for oxygen and carbon,

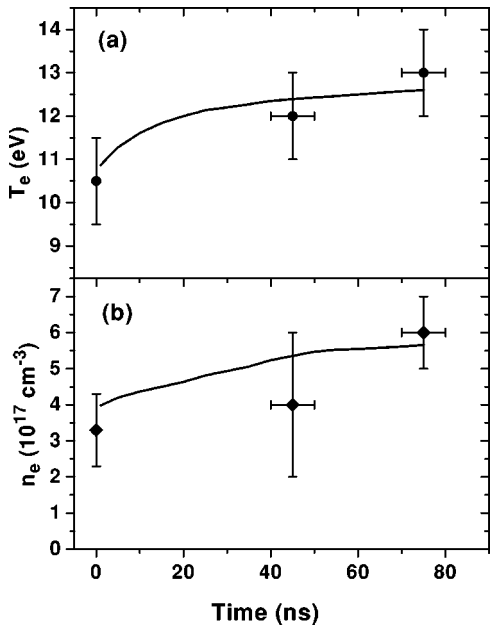

FIG. 5. (a) $T_e(t)$ used for the best-fit calculation (Fig. 4). Also shown are the data points obtained from Ref. [8]. (b) $n_e(t)$ used for the best-fit calculation, shown together with the data points for N_e calculated using the procedure described in Sec. III A.

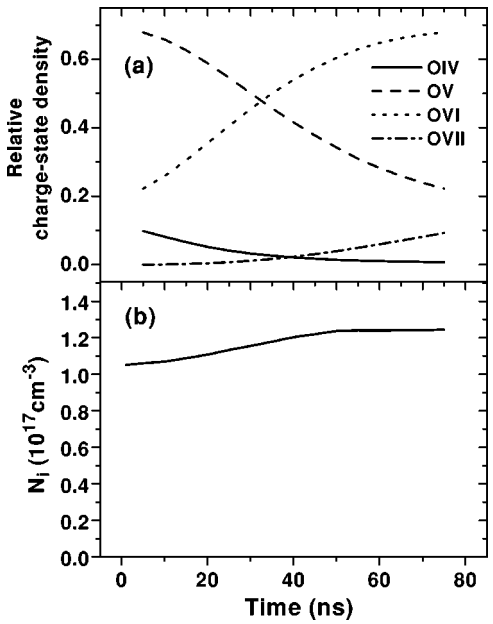

FIG. 6. (a) The charge-state composition history obtained from the best-fit calculation of γ(calc.) in Fig. 4. (b) The total ion-density history in the imploding plasma shell, obtained using $n_e(t)$ from Fig. 5, and the average ionic charge $Z(t)$, calculated by accounting for the contributions of both oxygen and carbon.

respectively. The ion density obtained was found to be in agreement to within $\sim$20% with the results given in Ref. [9], where the density was determined using the measured ion radial velocities and ionization times for the different charge states.

C. Error analysis

We now examine the uncertainty in the procedures described above for the determination of the electron density and the charge-state composition, by considering the uncertainties in the data and in the modeling. The contributions of the uncertainties in the data were found to be as follows: The error in Δn_u due to the error in the absolute calibration of the spectroscopic system was $\simeq$40%, resulting in an uncertainty of $\simeq$20% in the calculated value of N_e, but not affecting γ(expt.). The statistical error in Δn_u, due to the discharge irreproducibility, was $\sim$10%, resulting in an error $\Delta\gamma$(expt.) of $\sim$15%. The statistical uncertainty in the calculated ion-density N^{α}_{tot} due to the averaging over several upper levels j was $\sim$10%. For the calculations described in Sec. III A, the uncertainty in T_e as given in Ref. [8] was found to affect the uncertainties both in the composition and in the density. For the example given in Table I above, $\Delta T_e = 1.5$ eV resulted in variations of $\sim$30% and $\sim$20% in the values of N_e and the charge-state composition, respectively. An additional experimental uncertainty was in the time of each data point, such as those given in Table II, typically ± 5 ns.

The uncertainties in the CR modeling for the calculations discussed in Sec. III A include those due to the selection of the source functions, and due to the use of time-averaged values of χ^{α}. The effect of both contributions gives rise to an uncertainty of $\sim$10% in the value of N_e obtained. In the time-dependent calculations, the best-fitting procedure allowed for an independent examination of the sensitivity of γ(calc) to variations in $n_e(t)$, $T_e(t)$, and the initial charge-state composition, which in turn allowed for reliably determining these parameters. The resulting uncertainty in $n_e(t)$ was found to be $\sim$25%, and the uncertainty in the O VI relative density was $\sim$20%.

It was found that γ(calc.) is mostly sensitive to variations in $T_e(t)$, as demonstrated in Fig. 7, where calculations of γ(calc.) using different functions $T_e(t)$ are presented. Also given in this figure are the data points of T_e taken from Ref. [8] (also given in Fig. 5 in the present paper), the uncertainty in each being ± 1 eV. It is evident that much smaller variations in T_e, of up to ± 0.5 eV for the examples given, result in significant variations in γ(calc.). It can therefore be concluded that this high sensitivity of γ(calc.) to $T_e(t)$ allowed for two improvements in the determination of $T_e(t)$. First, it yielded a reduction in the uncertainty of each data point for T_e (as shown in Fig. 7), and it provided the time dependence of $T_e(t)$, rather than a simple interpolation of the data points.

IV. DISCUSSION

The time-dependent ion density obtained above [Fig. 6(b)], together with the known time-dependent radial position of the imploding-shell boundaries [Fig. 1(b)], allows for tracking the rise in time of the plasma mass within this shell. The mass obtained, together with the known time-dependent mass of the low-density plasma present ahead of the imploding shell, then allows for examining quantitatively the initial radial distribution of the gas mass.

The imploding-shell mass is calculated for the times t

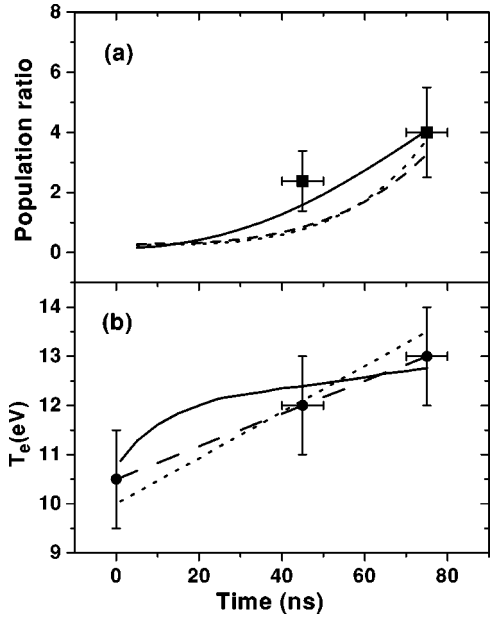

FIG. 7. An example of the effect of $T_e(t)$ on γ(calc.). (a) The ratio of the O VI $3p\ ^2P$ to the O V $2s\,3p\ ^3P$ level densities, calculated for the three functions $T_e(t)$ given in (b), shown together with the data points of γ(expt.). The solid, dashed, and dotted curves in (a) correspond to the solid, dashed, and dotted curves in (b), respectively. For comparison, also given in (b) are the data points of T_e as in Fig. 5(a).

$=490$, 535, and 570 ns, giving 2.6 ± 0.5, 3.2 ± 0.6, and 3.4 ± 0.6 μg/cm, respectively. At these times the imploding-shell width is $\simeq 1.5$ mm, while the entire plasma shell is ~ 6 mm wide [see Fig. 1(b)]. Based on other data of $n_i(r,t)$ presented in Ref. [9], it is also known that the mass of the low-density plasma (consisting of O II and O III) ahead of the imploding shell is only $\sim 30\%$ of the mass of the entire plasma column. In more detail, the mass of this plasma, for example at $t=490$ and $t=535$ ns, is 1.0 ± 0.3 and 0.8 ± 0.3 μg/cm, respectively. Evidently, the rise in the mass of the imploding shell is due to the sweeping of part of the dilute plasma into the imploding shell, where the dilute plasma is continuously provided with particles from the gas ahead of the plasma column.

Accounting for both the imploding-shell and the dilute plasma layer, the rise in the mass of the entire plasma obtained from these values is thus found to be small, $\sim 10\%$ between $t=490$ and 535 ns. This shows that the sweeping of new gas particles at the ionization front $R_{min}(t)$ is small. It can, therefore, be concluded that the plasma column has a nearly hollow geometry. Such an information on the initial gas profile in gas-puff *Z*-pinch plasmas is usually obtained from measurements using various ionization gauges prior to the high-voltage discharge.

A detailed discussion on the ionization dynamics and the energy balance for the entire plasma, and particularly on the mechanisms sustaining the propagation of the ionization wave, is given in Refs. [8,9].

V. SUMMARY

In summary, an analysis of spectral line intensities for a self-consistent, relatively highly accurate determination of the electron density, electron temperature, and ionic charge-state composition as a function of time and radial position in an imploding plasma is presented. The logical steps in such an analysis may be different for different experimental parameters. However, similar considerations can be applied to various conditions of plasmas that are not in ionization equilibrium and that are characterized by time-varying density, temperature, and composition.

ACKNOWLEDGMENTS

The authors wish to thank Yu. V. Ralchenko for helpful discussions on the atomic-physics modeling, and P. Meiri for his skilled technical assistance. This work was supported in part by the German-Israeli Project Cooperation foundation, and Sandia National Laboratories.

[1] H.R. Griem, *Plasma Spectroscopy* (McGraw-Hill, New York, 1964).
[2] N.R. Pereira and J. Davis, J. Appl. Phys. **64**, R1 (1988).
[3] D.D. Ryutov, M.S. Derzon, and M.K. Matzen, Rev. Mod. Phys. **72**, 167 (2000).
[4] E.J. Iglesias and H.R. Griem, Phys. Rev. A **38**, 301 (1988).
[5] Th. Wrubel, S. Buescher, and H.-J. Kunze, Plasma Phys. Controlled Fusion **42**, 519 (2000).
[6] Yu.V. Ralchenko and Y. Maron, J. Quant. Spectrosc. Radiat. Transf. **71**, 609 (2001).
[7] H.R. Griem, *Principles of Plasma Spectroscopy* (Cambridge University Press, Cambridge, UK, 1997), p. 235.
[8] L. Gregorian, G. Davara, E. Kroupp, V. A. Bernshtam, A. Starobinets, Yu. V. Ralchenko, and Y. Maron, Weizmann Institute Report No. WIS/22/02-June-DPP (unpublished).
[9] L. Gregorian, G. Davara, E. Kroupp, V.I. Fisher, A. Starobinets, V.A. Bernshtam, and Y. Maron, Weizmann Institute Report No. WIS/23/02-June-DPP (unpublished).
[10] M.E. Foord, Y. Maron, G. Davara, L. Gregorian, and A. Fisher, Phys. Rev. Lett. **72**, 3827 (1994).
[11] G. Davara, Ph.D. thesis, Feinberg Graduate School, Weizmann Institute of Science, 1995 (unpublished).
[12] G. Davara, L. Gregorian, E. Kroupp, and Y. Maron, Phys. Plasmas **5**, 1068 (1998).